PNAS

Supporting Information for

Polyubiquitin ligand-induced phase transitions are optimized by spacing between ubiquitin units

Sarasi K. K. Galagedera[1], Thuy P. Dao[1], Suzanne E. Enos[1], Antara Chaudhuri[1], Jeremy D. Schmit[2,*], and Carlos A. Castañeda[1,3,4,*]

* Corresponding Authors:
Jeremy D. Schmit schmit@phys.ksu.edu ; Carlos A. Castañeda, cacastan@syr.edu

This PDF file includes:

Other supporting materials for this manuscript include the following:

Dataset

A. Detailed Materials and Methods

Subcloning, Protein Expression, and Purification

Ub and Ub mutants were expressed in *Escherichia coli* NiCo21 (DE3) cells and purified using previously described procedure (1).

The genes encoding all HT6-Ub constructs (Table S4) were codon-optimized, synthesized, and cloned into pET24b (Novagen) by GenScript (NJ, USA). HT6-Ub constructs were grown in NiCo21 cells in Luria-Bertani (LB) broth with 50 mg/L kanamycin to OD_{600} of 0.6 (except for HT6$(GS)_{50}$Ub, which was grown to OD_{600} of 0.8-1.0), induced with 0.5 mM IPTG and expressed overnight at 37˚C. Then the cells were pelleted, frozen, and resuspended to lyse in 20 mL of 50 mM Tris buffer pH 8.0 with 1 mM PMSF, 1 mM $MgCl_2$, 1 mg/ml lysozyme and 25 µM Pierce universal nuclease. The lysate was centrifuged at 20 000 *g for 30 min, the supernatant was separated and loaded onto anion exchange column (Cytiva) and eluted with a gradient between 20 mM HEPES, 0.02 % NaN_3 buffer pH 7 and 20 mM HEPES, 0.02 % NaN_3 and 1 M NaCl buffer pH 7. Fractions containing HT6-Ub were collected and diluted 1:1 using 50 mM ammonium acetate pH 4.5. The resulting solution was centrifuged at 10 000 *g for 10 min, after which the supernatant was loaded onto a cation exchange column (Cytiva) and eluted with a gradient (Buffer A: 50 mM ammonium acetate pH 4.5, Buffer B: 50 mM ammonium acetate, 1 M NaCl pH 4.5). Fractions containing HT6-Ub were collected and dialyzed into 20 mM sodium phosphate buffer pH 6.8 with 0.5 mM EDTA and 0.02 % NaN_3 overnight. Finally, the fractions were concentrated using Amicon Ultra concentrators (10,000 MW cutoff) and stored at -80˚C until needed.

All M1-Ub4 constructs were expressed in *Escherichia coli* NiCo21 (DE3) cells in LB broth at 37˚C overnight. Then the cells were pelleted, frozen, and resuspended to lyse in 20 mL of 50 mM Tris buffer pH 8.0 with 1 mM PMSF, 1 mM $MgCl_2$, 1 mg/ml lysozyme and 25 µM Pierce universal nuclease. The lysate was centrifuged at 20 000 *g for 30 min, the supernatant was separated, and loaded onto the anion exchange column and the flowthrough was collected. The flowthrough was loaded onto the cation exchange column and eluted with a gradient (Buffer A: 50 mM ammonium acetate pH 4.5, Buffer B: 50 mM ammonium acetate, 1 M NaCl pH 4.5). The fractions containing M1-Ub4 were collected, concentrated, and buffer exchanged into 20 mM sodium phosphate buffer pH 6.8 with 0.5 mM EDTA and 0.02% NaN_3 using Amicon Ultra concentrators (10,000 MW cutoff) and stored at -80˚C until needed.

Full-length UBQLN2 and UBQLN2 450-624 were expressed and purified as described previously (2, 3). Briefly, the constructs were transformed into Rosetta 2 (DE3) pLysS *E. coli* cells and were grown in LB media with a final concentration of 50 mg/L kanamycin and 34 mg/L chloramphenicol to OD_{600} of 0.6-0.8, induced with 0.5 mM IPTG, and expressed overnight at 37˚C. Then the cells were pelleted, frozen, lysed, then purified via a "salting out" process, where NaCl was added to the spun down lysate to a final concentration of 0.5 - 1 M. The resulting UBQLN2 condensate phase was pelleted and then resuspended in cold 20 mM sodium phosphate buffer pH 6.8, with 0.5 mM EDTA & 0.02 % NaN_3. Leftover NaCl was removed through HiTrap desalting column (GE Healthcare), concentrated, and stored at -80 ˚C until needed.

Spectrophotometric Absorbance/Turbidity Measurements

Turbidity assays were generally performed as described in (2). Protein samples were prepared by mixing different ratios of UBQLN2 450C (or full length UBQLN2) and Ub mutants/HT6-Ub/M1-Ub4 constructs (the initial concentrations of the protein stocks were doubled compared to the sample concentrations) in cold 20 mM sodium phosphate buffer pH 6.8 with 0.5 mM EDTA and 0.02 % NaN_3. Then, cold 400 mM NaCl in 20 mM sodium phosphate buffer pH 6.8 with 0.5 mM EDTA and 0.02 % NaN_3 was added in a 1:1 ratio. Both solutions were kept on ice for at least 5 min before mixing. Absorbance at 600 nm was monitored as a function of temperature using a Cary 3500 UV/Vis spectrophotometer (Agilent) using a temperature ramp rate of 1 ˚C/min increasing from 15 ˚C to 60 ˚C (for HT6-Ub, HT6-Ub mutants & M1-Ub4 constructs) and 25 ˚C to 60 ˚C (for Ub mutants). Several full-length UBQLN2 assays used a temperature range from 4 ˚C to 60 ˚C. Net absorbance values were recorded after subtracting the absorbance value from the reference buffer.

Cloud Point Temperature Curve Measurements

The phase boundary for UBQLN2 LCST (lower critical solution temperature) phase transitions at specific concentrations of ligand and protein were determined from turbidity assays as described above (2). The ligand hub concentrations were chosen to cover as wide a range as possible. Cloud point temperature values were determined by fitting a Four Parameter Logistic Regression model to the data using MATLAB R2019b:

$$y = d + \frac{(a-d)}{1+\left(\frac{x}{c}\right)^b}$$

where *a* and *d* are minimum and maximum absorbance values, *b* is the Hill slope reflecting steepness of the phase transition and *c* is the temperature at the inflection point or the cloud point

temperature (T_{cp}). T_{cp} values were used to define the cloud point temperature curve as a function of ligand:protein ratio (ligand refers to Ub mutants/HT6-Ub/M1-Ub4 and protein to either UBQLN2 450C or full length UBQLN2). Here, results were averaged from data collected using a total of six trials with proteins from two separate protein preps.

Calculations of Dilute and Dense Phase Concentrations

Samples were prepared on ice to contain 60 µL of 240 µM UBQLN2 450C, 10 µM of UBQLN2 450C labeled with Alexa Fluor 488, and 250 µM of HT6-(GS/PA)x-Ub in 20 mM NaPhosphate, 200 mM NaCl, 0.1 mM TCEP, and 0.5 mM EDTA (pH 6.8). Samples were incubated in microcentrifuges that had been equilibrated at 5, 15, 25, 35, 45 and 55 ºC for 10 minutes, then centrifuged at 10000 x g for 5 minutes at the set temperatures. Without disrupting the pellet, as much of the supernatant as possible was transferred to a new tube. 8 µL of 8 M urea solution was added to the pellet. Tube containing pellet and urea was incubated for 1 hour at room temperature, vortexed and centrifuged. The volume of the mixture was determined by pipetting with a P10. The dense phase volume was determined by subtracting the total volume by 8 µL of urea added. Fluorescence reading at excitation of 490 nm and emission at 525 nm (for Alexa Fluor 488/UBQLN2) were recorded on a SpectraMax i3x plate reader (Molecular Devices). Dense and dilute phase concentrations were determined with a standard curve for multiple concentrations of UBQLN2 mixed with UBQLN2 labeled with Alexa Fluor 488.

NMR Experiments

All NMR data were collected at 25˚C using a Bruker Avance III 800 MHz spectrometer equipped with TCI cryoprobe. Protein solutions were prepared in a 20 mM NaPhosphate buffer (pH 6.8) with 0.5 mM EDTA, 0.02 % NaN_3, and 5 % D_2O. Data collected were processed using NMRPipe (4) and analyzed using CCPNMR 2.5.2 (5). Chemical shift perturbations (CSPs) were quantified as follows:

$$CSP = \Delta\delta = \sqrt{(\Delta\delta_H)^2 + (\Delta\delta_N/5)^2}$$

Here $\Delta\delta_H$ and $\Delta\delta_N$ are the differences in ^{1}H and ^{15}N chemical shifts in ppm, respectively.

^{15}N Relaxation Experiments

Longitudinal (R_1) and transverse (R_2) ^{15}N relaxation rates were measured for 200 µM samples of Ub and different HT6-Ub constructs using previously described protocols (1, 6). Relaxation inversion recovery periods for R_1 experiments were 4 ms (*2), 600 ms (*2), and 1000 ms (*2), using an interscan delay of 2.5 s. Total spin-echo durations for R_2 were 8 ms (*2), 32 ms (*2), 48

ms (*2), 64 ms (*2), and 80 ms (*2) using an interscan delay of 2.5 s. All relaxation experiments were acquired using spectral widths of 12 and 24 ppm in the ^{1}H and ^{15}N dimensions, respectively, with corresponding acquisition times of 110 ms and 31 ms. Relaxation rates were calculated by fitting peak heights to a mono-exponential decay using RELAXFIT (7). The average R_1 and R_2 values >63 residues in secondary structure elements of Ub were reported.

NMR Titration Experiments and K_d Determination

^{1}H-^{15}N SOFAST-HMQC experiments were used for titrations of different Ub mutants/ HT6-Ub/ M1-Ub4 constructs into UBQLN2 UBA samples. Unlabeled protein ligand (Ub mutants/ HT6-Ub constructs/ M1-Ub4 constructs) was titrated into 100 μM samples of ^{15}N-labeled protein (usually UBQLN2 UBA domain) and the binding was monitored as a function of different ligand:protein ratios. At each titration point, it was assumed that the CSP for each backbone amide was a weighted average between the free ($\Delta\delta$=0) and ligand-bound states ($\Delta\delta$= $\Delta\delta_{max}$). Therefore, the CSP reports on the relative population of the ligand-bound state, such that $\Delta\delta = \Delta\delta_{max} * [PL]/[Pt]$, where [PL] and [$P_t$] represent the ligand-bound and the total UBA protein concentrations, respectively. Data fitting for each amide was performed using an in-house MATLAB program, with the assumption of a single-site binding model (1:1 stoichiometry). The equation for single-site binding for fast exchange is as follows:

$$[PL]/[Pt] = ([Pt] + [Lt] + Kd - \sqrt{([Pt] + [Lt] + Kd)^2 - 4[Pt][Lt]})/2[Pt]$$

Here, $[Pt]$ and $[Lt]$ are total protein and ligand concentrations, respectively, and K_d is the binding affinity. Reported K_d values for each titration experiment were averages of residue-specific K_d values. The errors reflect the standard deviation of these values.

SEC-MALS-SAXS Experiments

SAXS was performed at BioCAT (beamline 18ID at the Advanced Photon Source, Chicago) with in-line size exclusion chromatography (SEC-SAXS) to separate sample from aggregates and other contaminants thus ensuring optimal sample quality and multiangle light scattering (MALS), dynamic light scattering (DLS) and refractive index measurement (RI) for additional biophysical characterization (SEC-MALS-SAXS). Sample was loaded onto a Superdex 200 Increase 10/300 GL column (Cytiva) run by 1260 Infinity II HPLC (Agilent Technologies) at 0.6 ml/min. The flow passed through (in order) the Agilent UV detector, a MALS detector and a DLS detector (DAWN Helios II, Wyatt Technologies), and an RI detector (Optilab T-rEX, Wyatt). The flow then went through the SAXS flow cell. The flow cell consists of a 1.0 mm ID quartz capillary with ~20 μm walls. A coflowing buffer sheath is used to separate the sample from the capillary walls, helping

prevent radiation damage (8, 9). Scattering intensity was recorded using a Pilatus3 X 1 M (dectris) detector which was placed 3.6 m from the sample giving access to a q-range of 0.003 $Å^{-1}$ to 0.35 $Å^{-1}$. 0.5 s exposure was acquired every 2 s during elution, and data were reduced using BioXTAS RAW 2.1.1 (10). Buffer blanks were created by averaging regions flanking the elution peak (see Fig S4, 7, 11) and subtracted from exposure selected from the elution peak to create the I(*q*) vs. *q* curves used for subsequent analysis. Molecular weights and hydrodynamic radii were calculated from the MALS and DLS data respectively using ASTRA 7 software (Wyatt) (11, 12). Additionally, R_g and I(0) values were obtained using the entire q-range of the data by calculating the distance distribution functions, P(*r*) vs. r, using GNOM (13). All SEC-MALS-SAXS parameters for data collection and analysis can be found in Dataset 1A and 1B.

Representative structure determination of ligand hubs from SAXS and SASSIE

We employed SASSIE (14) to generate structural ensembles for various HT6-Ub and M1-Ub4 ligand hubs with different linker lengths. Starting PDB structure files were built using AlphaFold2 (15). For M1-Ub4 ligands, we used the monomer configuration generator module of SASSIE to initially build 30,000 structures. As HT6-Ub ligands are tetrameric complexes, we used the Complex configuration generator module to build 30,000 structures. Monte Carlo moves about the ϕ/Ψ backbone torsion angles were permitted only for selected residues (i.e., only these residues were deemed flexible in the structures) as denoted in Table S5, and each move was restricted to a maximum of 30 degrees. Trial structures were rejected if there were Cα-atom steric clashes within 3 Å. This yielded around 13,000 – 21,000 sterically-allowed structures (Table S5). X-ray scattering curves were then calculated for each of these structures. The single structure with the lowest χ^2 (in comparison to the experimental X-ray scattering curve for the specific ligand hub) was then selected as the representative structure as shown in Fig. 2 and 4.

B. Theory for ligand-mediated phase transitions

Solution Free Energy

To reconcile the observation that (mono)Ub and polyUb inhibit and promote phase separation, respectively, we developed a theoretical framework that is equivalent to the polyphasic linkage concepts introduced by Wyman and Gill (16, 17). Differences exist as the original formalism describes a multivalent central molecule (e.g., sickle cell hemoglobin with multiple binding sites) that undergoes a ligand-induced phase transition, where the ligand is monovalent (e.g., O_2). In our system, the multivalent molecule is polyUb (with multiple UBA binding sites) that does not phase separate on its own. Here, polyUb interacts with UBQLN2 (with a single Ub binding site) that is independently capable of phase separating. Thus, the role of the "driver" molecule (which sets the reference concentration) is inverted between the two formalisms.

The first requirement of the model is that it must capture the binding equilibrium of Ub and UBQLN2 into higher order complexes. We begin by writing down the free energy of the dilute state, which we denote with the index V = "vapor":

(Eq. S1)

$$F_V = c_{h,V}\left(\ln\frac{c_{h,V}}{c_0} - 1 + f_h\right) + c_{d,V}\left(\ln\frac{c_{d,V}}{c_0} - 1 + f_d\right) + \sum_{n=1}^{N} c_{n,V}\left(\ln\frac{c_{n,V}}{c_0} - 1 + f_n\right) + \mu_h\left(c_{H,V} - c_{h,V} - \sum_{n=1}^{N} c_{n,V}\right) + \mu_d\left(c_{D,V} - c_{d,V} - \sum_{n=1}^{N} n\, c_{n,V}\right)$$

Here $c_{h,V}$ and $c_{d,V}$ are the concentrations of hub and driver molecules in the monomer state, respectively (i.e., not bound to any other hub or driver molecule). N is the number of driver molecules that a hub can bind (N=4 in the case of Ub4) and $c_{n,V}$ is the concentration of hubs that are bound to n driver molecules ("n-mers"). f_i is the free energy of species i and $c_i\left(\ln\frac{c_i}{c_0} - 1\right)$ is the mixing entropy of that species, where c_0 is a reference concentration. The chemical potentials μ_h and μ_d serve as Lagrange multipliers to ensure that the concentration of molecules in the monomer and n-mer states add up to the total concentration of hubs, $c_{H,i}$, and driver molecules, $c_{D,i}$. (In our notation, the capital index (e.g., H, D) indicates the total concentration while the lowercase (e.g., h, d) indicates the monomer state).

The free energy of the dense state (denoted with the subscript L = "liquid") has a similar form:

(Eq. S2)

$$F_L = c_{h,L}\left(\ln\frac{c_{h,L}}{c_0} - 1 + f_h + s_h\right) + c_{d,L}\left(\ln\frac{c_{d,L}}{c_0} - 1 + f_d + s_d\right) + \sum_{n=1}^{N} c_{n,L}\left(\ln\frac{c_{n,L}}{c_0} - 1 + f_n + s_n\right) + \mu_h\left(c_{H,L} - c_{h,L} - \sum_{n=1}^{N} c_{n,L}\right) + \mu_d\left(c_{D,L} - c_{d,L} - \sum_{n=1}^{N} n\, c_{n,L}\right)$$

Where s_i is the energy to transfer species i from the dilute, vapor (V) state to the liquid (L) state (e.g. s_h is the energy to transfer the hub from the vapor to liquid state).

Chemical and Partitioning Equilibrium

Minimizing F_V and F_L with respect to c_i we find expressions for each of the species concentrations in the vapor phase:

(Eq. S3)

$$c_{h,V} = c_0 e^{-f_h + \mu_h}$$
$$c_{d,V} = c_0 e^{-f_d + \mu_d}$$
$$c_{n,V} = c_0 e^{-f_n + \mu_h + n\mu_d}$$

And in the liquid phase:

(Eq. S4)

$$c_{h,L} = c_0 e^{-f_h - s_h + \mu_h}$$
$$c_{d,L} = c_0 e^{-f_d - s_d + \mu_d}$$
$$c_{n,L} = c_0 e^{-f_n - s_n + \mu_h + n\mu_d}$$

The expressions for the monomers in the vapor phase can be rearranged to find expressions for the chemical potentials:

(Eq. S5)

$$\mu_h = \ln \frac{c_{h,V}}{c_0} + f_h$$
$$\mu_d = \ln \frac{c_{d,V}}{c_0} + f_d$$

These expressions can be used with Eqs. S3 and S4 to obtain the conditions for (unbound) monomer phase partitioning:

(Eq. S6)

$$c_{h,V} = c_{h,L} e^{s_h}$$
$$c_{d,V} = c_{d,L} e^{s_d}$$

Similarly, the chemical potentials can be substituted in the expressions for the n-mer concentrations:

(Eq. S7)

$$c_{n,V} = \frac{c_{h,V} c_{d,V}^n}{c_0^n} e^{-(f_n - f_h - n f_d)}$$
$$= \frac{c_{h,V} c_{d,V}^n}{k_{n,V}}$$

Where $k_{n,V}$ is the dissociation constant for the formation of n-mers in the dilute (vapor) phase.

Similarly, in the dense (liquid) phase we find:

(Eq. S8)

$$c_{n,L} = \frac{c_{h,L} c_{d,L}^{n}}{c_0^{n}} e^{-(f_n - f_h - n\, f_d) - (s_n - s_h - n\, s_d)}$$
$$= \frac{c_{h,L} c_{d,L}^{n}}{k_{n,L}}$$

where

(Eq. S9)

$$k_{n,L} = k_{n,V} e^{(s_n - s_h - n s_d)}$$
$$k_{n,L} = k_{n,V} e^{\Delta s}$$

Note that if the transfer free energy of an n-mer is given by the sum of its parts such that $s_n = s_h + n s_d$ then the dissociation constants are identical in each phase. Therefore, Δs, is a parameter that describes how oligomerization (hub-driver binding) modifies the interaction with the fluid (driver-only fluid). However, if the bonding constraints within the n-mer perturb the interactions with the surrounding phase, the oligomerization equilibrium will be different between the phases (Δs will be non-zero).

The above formulation ensures that binding equilibria are satisfied in each phase and that the chemical potentials for each species are equal across phases.

Our next task is to determine a condition for the onset of phase separation. At the onset, we can consider the dense phase to be infinitesimally small so that all of the proteins are in the dilute (vapor) phase. Thus, $c_{H,V}$ and $c_{D,V}$ are equal to the total protein concentrations, which can be used with Eq. S7 to determine the monomer concentration ($c_{h,V}$ and $c_{d,V}$ (as described below)). These concentrations, in turn, can be used with Eq. S8 to find the monomer concentrations in the infinitesimal droplet. Next these concentrations are used with Eq. S9 to find the concentration of n-mers in the dense phase.

Saturated Solution Condition

To assess whether these concentrations represent a subsaturated or supersaturated solution we examine the total concentration of the driver molecules in the dense phase. When polymers phase separate, the mass concentration of the dense phase is insensitive to the molecular weight (or equivalently the polymerization number) of the individual molecules (18). This is because the microscopic interactions and mesh structure of the phase are both much smaller than the molecules. In agreement with this expectation, the concentration of UBQLN2 molecules in the dense phase is nearly constant regardless of whether the UBQLN2 are monomers (i.e., unbound UBQLN2) or oligomerized by a hub (19). Experimentally, we tested this for 450-624 in the presence of a few HT6-Ub ligands (Fig. S10A). Therefore, we adopt, as the criteria for phase separation, the condition that the total concentration of UBQLN2 in the dense phase is equal to the concentration of the UBQLN2-only fluid (i.e. in a UBQLN2-only phase separating solution):

(Eq. S10)

$$c_{d,L} + \sum_n n\, c_{n,L} = c_{D,L}$$

where the total concentration $c_{D,L}$ is taken to be the constants $c_{D,L}$ = 10 mM for 450C and $c_{D,L}$ = 2 mM for full length UBQLN2 (19). This step marks a departure from the Wyman and Gill formalism (17) in that we have used the concentration of UBQLN2 to set the reference concentration of the dense phase. This is necessary because the concentration of the pure polyUb fluid (polyUb alone in the dense phase) is not experimentally measurable.

An important insight from Eq. S10 is that hub molecules facilitate phase separation by lowering the chemical potential of driver molecules in the dense phase. This is most easily seen by examining the unbound driver chemical potentials in the two limiting cases:

- In a sub-saturated solution, the UBQLN2 concentration will add up to less than the pure UBQLN2 fluid: $c_{d,L} + \sum_n n\, c_{n,L} < c_{D,L}$. In this case, the dense phase will collapse to fill the voids and optimize the UBQLN2-UBQLN2 contacts. After this collapse, the monomer (unbound driver) concentration in the dense phase will increase such that the chemical potential in the dense phase is greater than the dilute phase: $\ln\frac{c_{d,V}}{c_0} < \ln\frac{c_{d,L}}{c_0} + s_d$. This will drive the monomers (unbound drivers) to leave the dense phase, causing it to shrink.

- Conversely, in a supersaturated solution we would find $c_{d,L} + \sum_n n\, c_{n,L} > c_{D,L}$ implying that the driver molecules are packed too close together. In this case the dense phase will expand, lowering the concentration of monomers. Again comparing the resulting chemical potentials of the monomers we find $\ln\frac{c_{d,V}}{c_0} > \ln\frac{c_{d,L}}{c_0} + s_d$, which will drive additional monomers (unbound complexes) to enter the dense phase.

Therefore, the condition for the onset of phase separation is when Eq. S10 is satisfied and the monomer concentrations satisfy

(Eq. S11)

$$\ln\frac{c_{d,V}}{c_0} = \ln\frac{c_{d,L}}{c_0} + s_d$$

Which is equivalent to Eq. S6.

In the absence of hubs ($c_{D,L} = c_{d,L}$), this expression gives Eq. 3 from the main text:

(Eq. S12)

$$\frac{c_{sat}}{c_{D,L}} = e^{s_d}$$

Temperature Dependence of Phase Separation

The temperature dependence of s_d is modeled by fitting the experimental cloud point temperatures to the quadratic function:

(Eq. S13)

$$c_{sat} = a(T - T_c)^2 + c_c$$

The best fit parameters are shown in Fig. S10B. Combining this with our previous result (Eq. S12) we have:

$$e^{s_d} = \frac{c_{sat}}{c_{D,L}}$$

(Eq. S14)

$$e^{s_d} = \frac{a(T - T_c)^2 + c_c}{c_{D,L}}$$

Next, we express our condition for phase separation in terms of s_d:

(Eq. S15)

$$c_{D,L} = c_{d,L} + \sum_n n\, c_{n,L}$$

$$c_{D,L} = c_{d,L} + \sum_n n \frac{c_{h,L} c_{d,L}^n}{k_{n,L}}$$

Using Eqs. S6 and S9 this becomes

(Eq. S16)

$$c_{D,L} = c_{d,V} e^{-s_d} + c_{h,V} e^{-s_h} \sum_n n \frac{\left(c_{d,V} e^{-s_d}\right)^n}{k_{n,V} e^{\Delta s}}$$

$$1 = \frac{c_{d,V}}{c_{sat}} + \frac{c_{h,V} e^{-s_h}}{c_{D,L}} \sum_n n \frac{\left(\frac{c_{d,V} c_{D,L}}{c_{sat}}\right)^n}{k_{n,V} e^{\Delta s}}$$

Finally, to reduce the number of free parameters in the model, we make the approximation that Δs is independent of n and obtain:

(Eq. S17)

$$1 = \frac{c_{d,V}}{c_{sat}} + \frac{c_{h,V} e^{-s_h - \Delta s}}{c_{D,L}} \sum_n n \frac{\left(\frac{c_{d,V} c_{D,L}}{c_{sat}}\right)^n}{k_{n,V}}$$

We refer to the quantity $s_h + \Delta s$ as the "inclusion energy". It accounts for two detrimental effects from transferring an n-mer to the dense phase. The first is the repulsive solvation energy of the hub and the second is the constraints preventing the bound drivers from attaining their optimal interactions with the fluid. This inclusion energy is the only free parameter in Eq. S17.

Calculation of Cloud Point Curves

Comparison between theory and experiment is complicated by the fact that Eq. S17 depends on the monomer (unbound) concentrations c_d and c_h, which are not readily known from

experiments. These quantities can be determined from the total concentrations as follows. First, we construct the partition function of a hub in the vapor phase:

(Eq. S18)

$$Q_h = 1 + \sum_{n=1}^{N} \frac{c_d^n}{k_{n,V}}$$

Where we approximate the equilibrium constants by assuming independent sites such that $k_{n,V} = k_0^n / {}_n^N C$, where k_0 is the dissociation constant between monoubiquitin and UBQLN2 at 25°C (Table S1) and ${}_n^N C$ is a binomial coefficient accounting for the multiplicity of binding. From the partition function we obtain an expression for the average number of bound drivers per hub

(Eq. S19)

$$\langle n \rangle = \frac{1}{Q_h} \sum_{n=1}^{N} n \frac{c_d^n}{k_{n,V}}$$

With this expression we can write an equation for c_d in terms of the total concentrations:

(Eq. S20)

$$c_D = c_d + \langle n \rangle c_H$$

The left side of c_d monotonically increases for positive values of c_d, meaning that there is only one root within the range $0 < c_d \leq c_D$ that can be readily found numerically. With c_d known, c_h is obtained from the statistical weight of the monomer term in the partition function

(Eq. S21)

$$c_h = \frac{c_H}{Q_h}$$

The quantities c_h and c_d are inserted into Eq. S17, along with Eq. S13, which is numerically solved for the onset temperature.

C. SI Figures

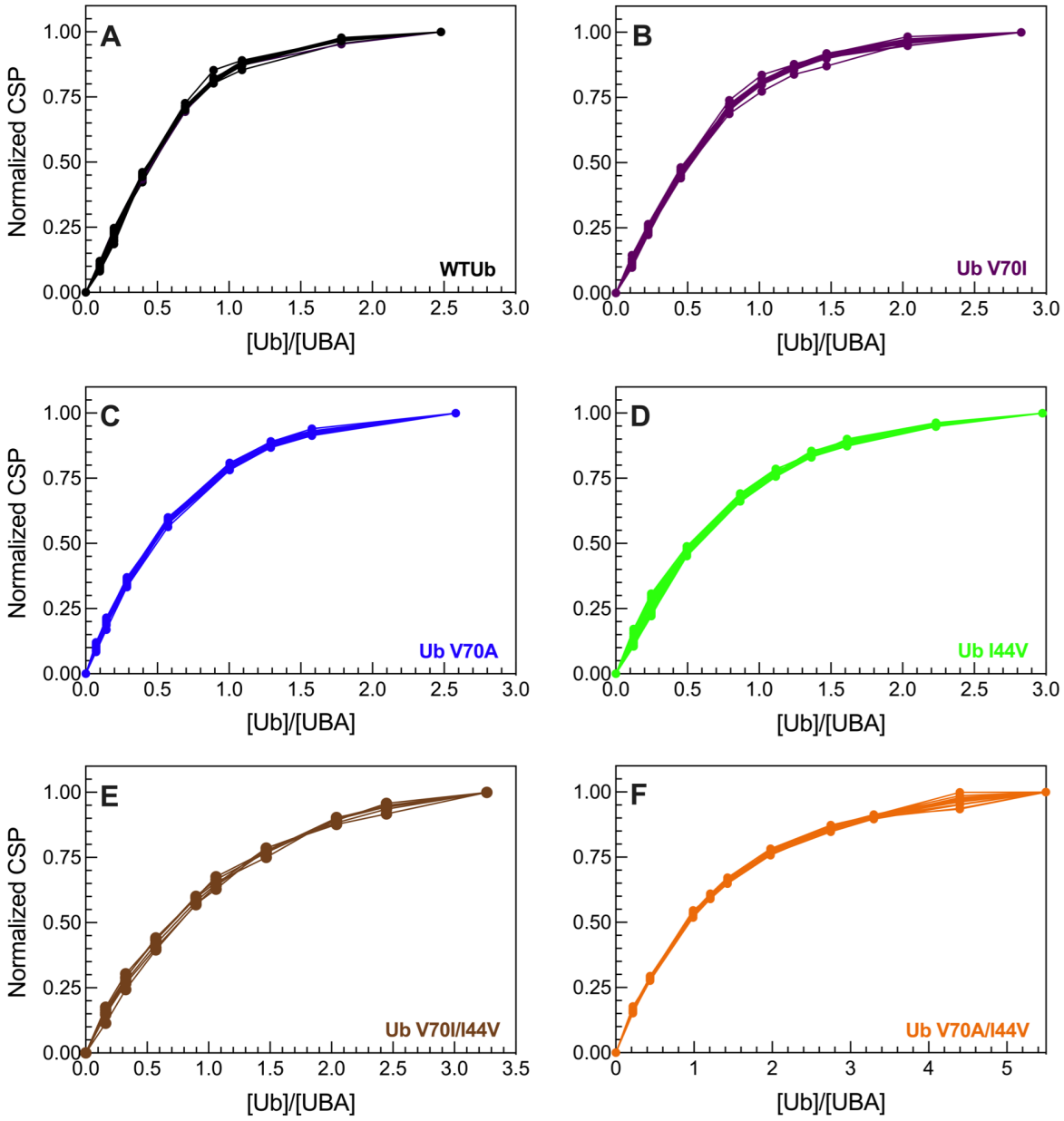

Figure S1. Residue-specific normalized backbone amide titration curves for 100 μM ^{15}N UBQLN2 UBA resonances after titrating 0-250 μM of (A) WT Ub [22 amino acid resonances], (B) Ub V70I [21], (C) Ub V70A [17], (D) Ub I44V [23], (E) Ub V70I/I44V [6], & (F) Ub V70A/I44V [18]. See Table S1 for a list of specific amino acid resonances used.

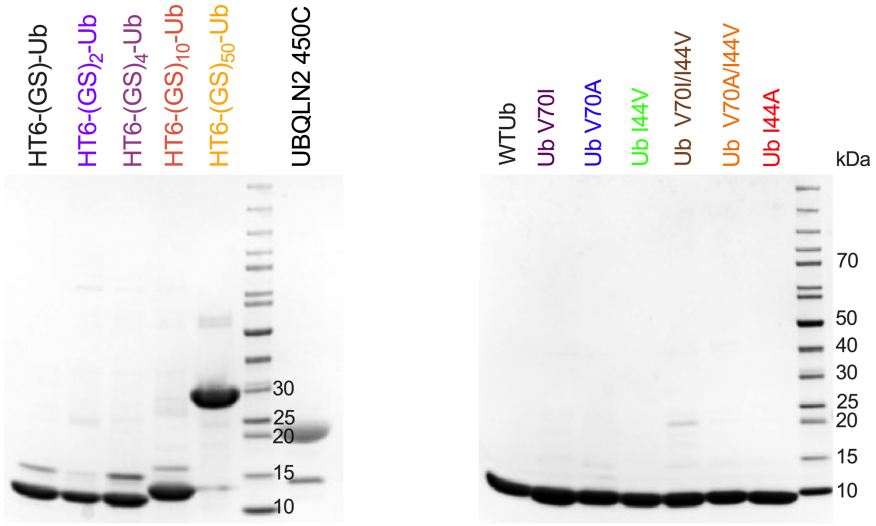

Figure S2. Representative Mini-PROTEAN TGX Precast gel images of (A) HT6-Ub and UBQLN2 450C, and (B) Ub mutants used in this study.

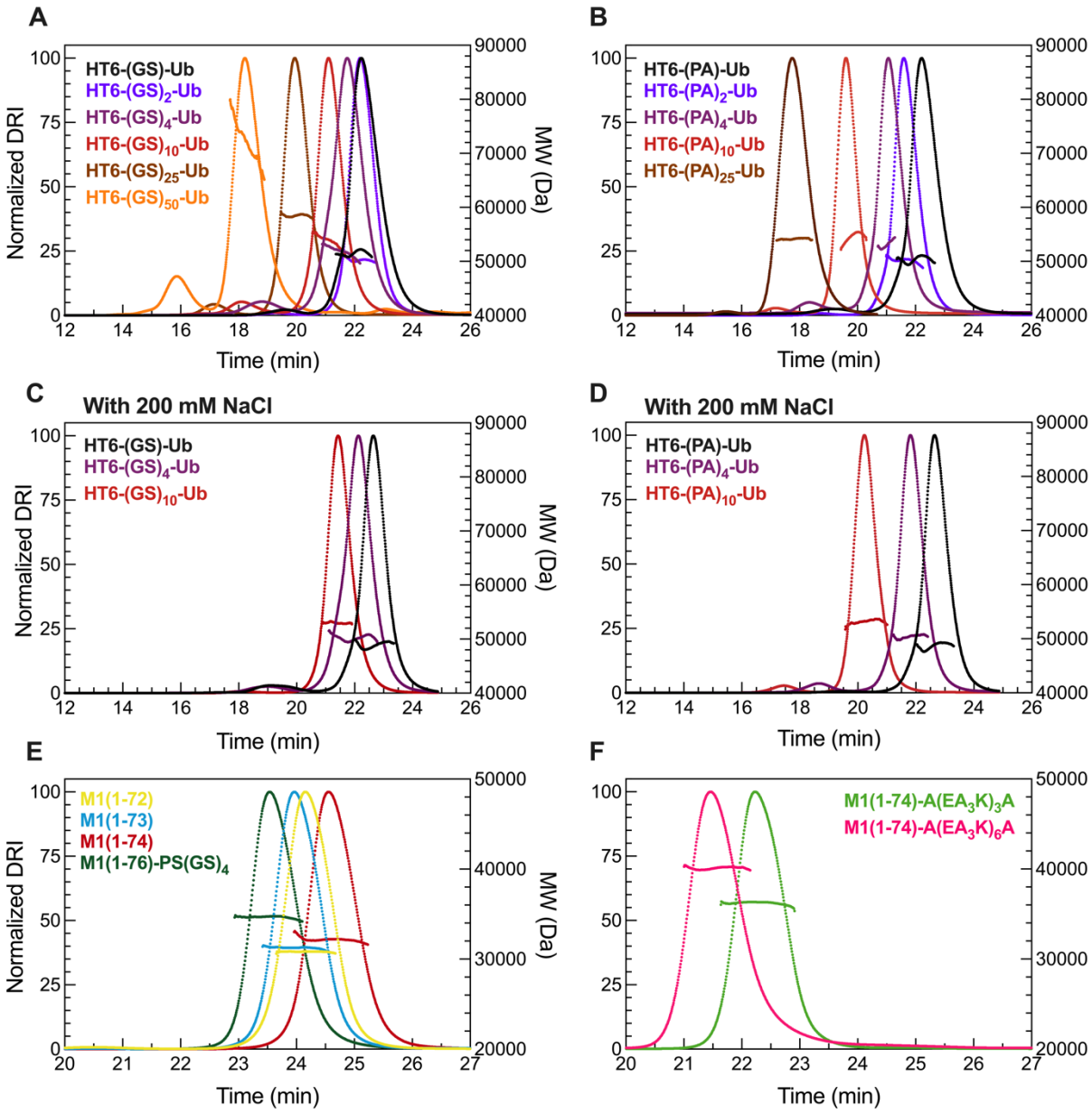

Figure S3. SEC-MALS profiles for various Ub4 ligand hubs used in this study. As expected, HT6-Ub is a tetramer. The molecular weight (MW) of (A) HT6-$(GS)_x$-Ub (B) HT6-$(PA)_x$-Ub (E) M1-linked Ub4 chains, and (F) M1-linked Ub4 chains with long Ub-Ub linkers were determined using SEC-MALS experiments. To test for the effect of salt on HT6-Ub oligomerization, we collected represented SEC-MALS profiles for (C) HT6-$(GS)_x$-Ub and (D) HT6-$(PA)_x$-Ub hubs. For all profiles collected above, the observed MW values are consistent with the expected MW of these constructs.

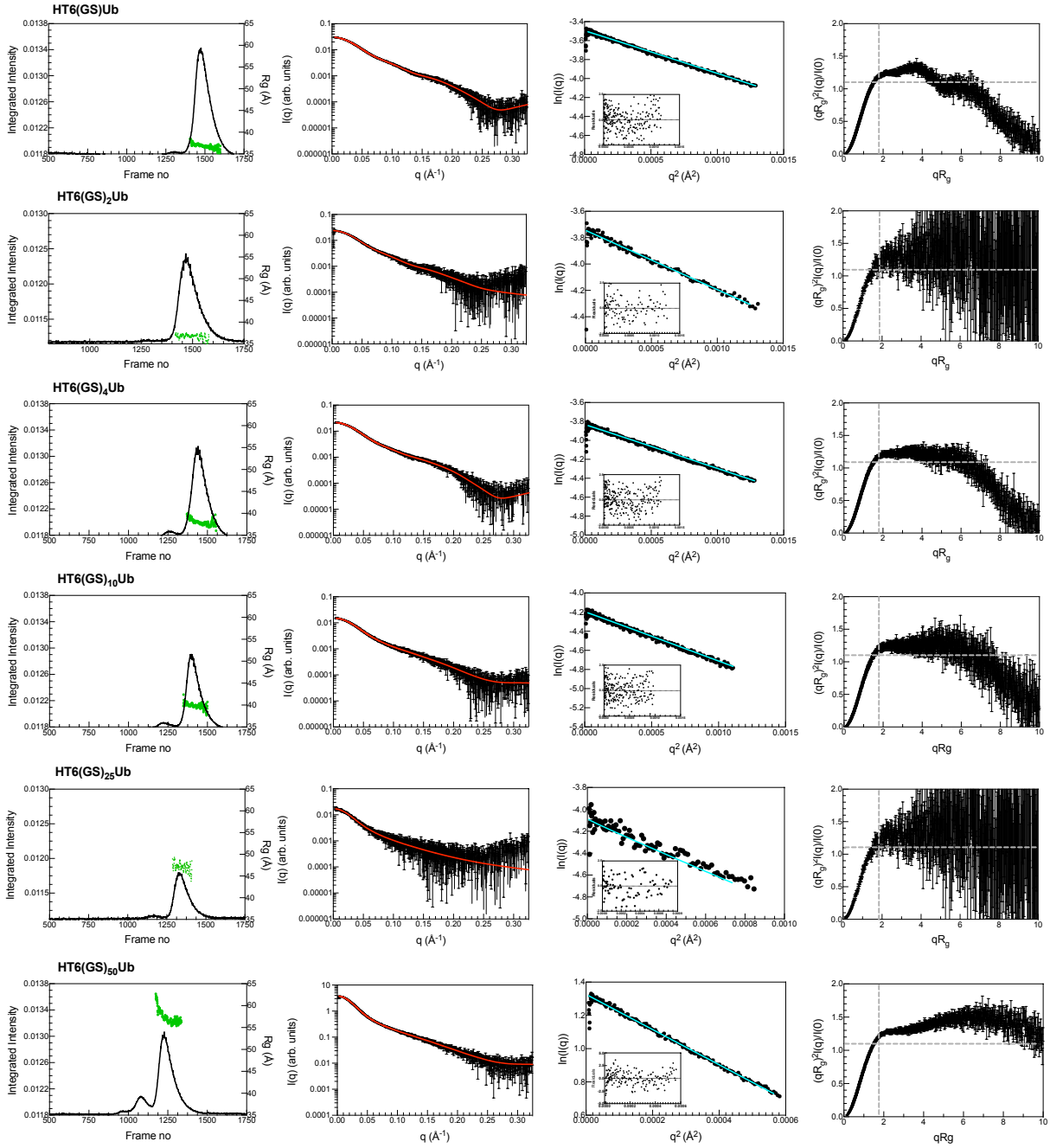

Figure S4A. (Left) SEC-SAXS profiles for HT6-(GS)-Ub, HT6-$(GS)_4$-Ub, HT6-$(GS)_{10}$-Ub, & HT6-$(GS)_{50}$-Ub. I(q) vs. q scattering curves (middle left) determined from frames (1438-1475) HT6-(GS)-Ub, (1453-1465) HT6-$(GS)_2$-Ub, (1448-1500) HT6-$(GS)_4$-Ub, (1423-1469) HT6-$(GS)_{10}$-Ub, (1322-1325) HT6-$(GS)_{25}$-Ub & (1165-1399) HT6-$(GS)_{50}$-Ub on the corresponding SEC-SAXS profiles (left). Red line in the I(q) profile indicates fit from P(r) analysis (see Fig. 2C). Cyan line in the Guinier plot (middle right) is the linear fit of ln(I(q)) vs. q^2, while inset shows residuals of fit. Dimensionless Kratky plots (right) include dashed lines to indicate where a globular protein would peak. Increase in polyUb chain flexibility from top (HT6-(GS)-Ub) to bottom (HT6-$(GS)_{50}$-

Ub) is indicated by shifts in the peak position up and to the right of the globular peak and larger plateaus in the higher q region.

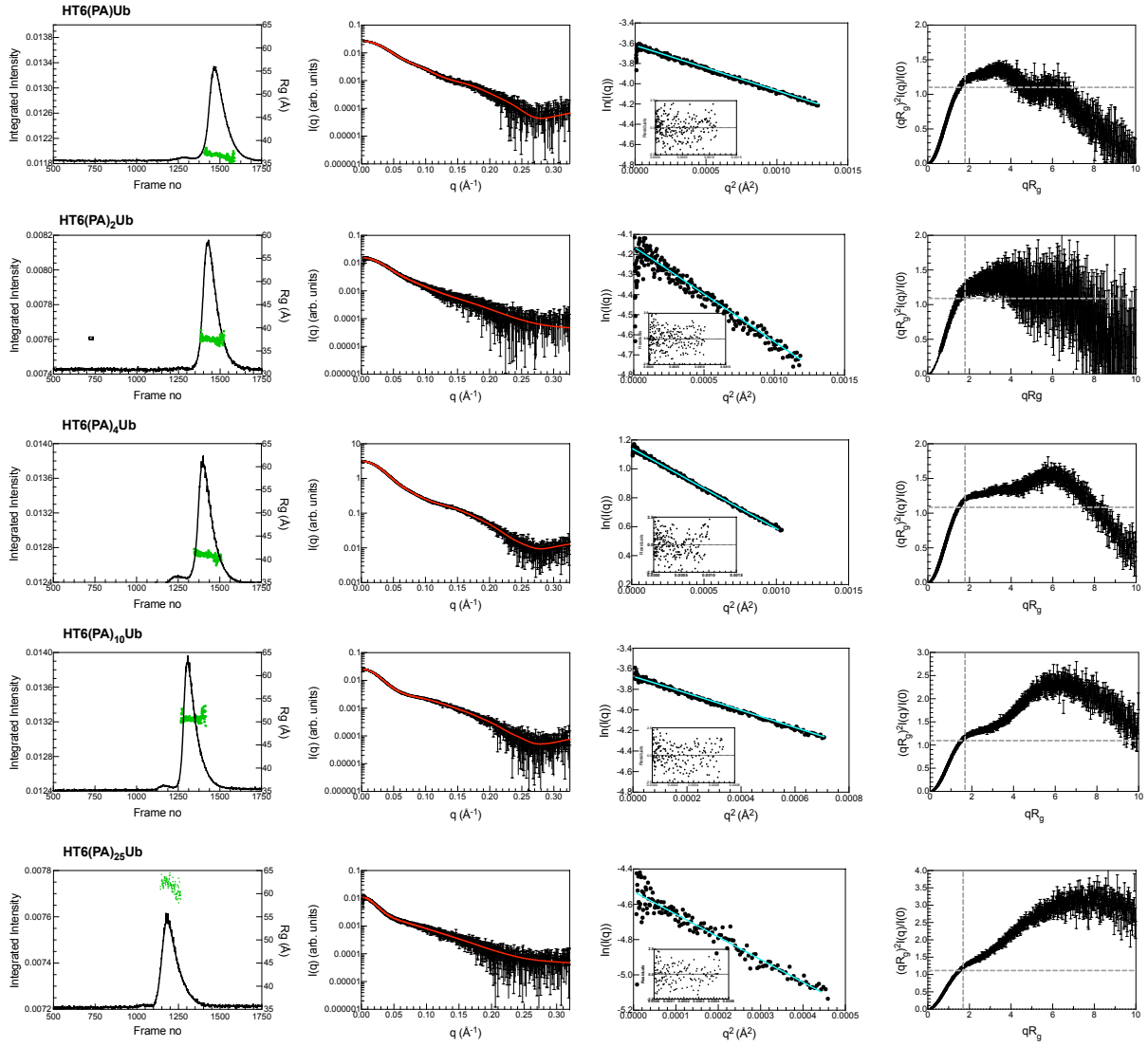

Figure S4B. SEC-SAXS profiles for HT6-(PA)-Ub, HT6-$(PA)_2$-Ub, HT6-$(PA)_4$-Ub, HT6-$(PA)_{10}$-Ub & HT6-$(PA)_{25}$-Ub. I(q) vs. q scattering curves (middle left) determined from frames (1478-1502) HT6-(PA)-Ub, (1425-1430) HT6-$(PA)_2$-Ub, (1452-1476) HT6-$(PA)_4$-Ub, (1352-1376) HT6-$(PA)_{10}$-Ub & (1183-1195) HT6-$(PA)_{25}$-Ub on the corresponding SEC-SAXS profiles (left). Red line in the I(q) profile indicates fit from P(r) analysis (see Fig. 2C). Cyan line in the Guinier plot (middle right) is linear fit of ln(I(q)) vs. q^2, while inset shows residuals of fit. Dimensionless Kratky plots (right) include dashed lines to indicate where a globular protein would peak. Increase in polyUb chain flexibility from top (HT6-(PA)-Ub) to bottom (HT6-$(PA)_{25}$-Ub) is indicated by shifts in the peak position up and to the right of the globular peak and larger plateaus in the higher q region.

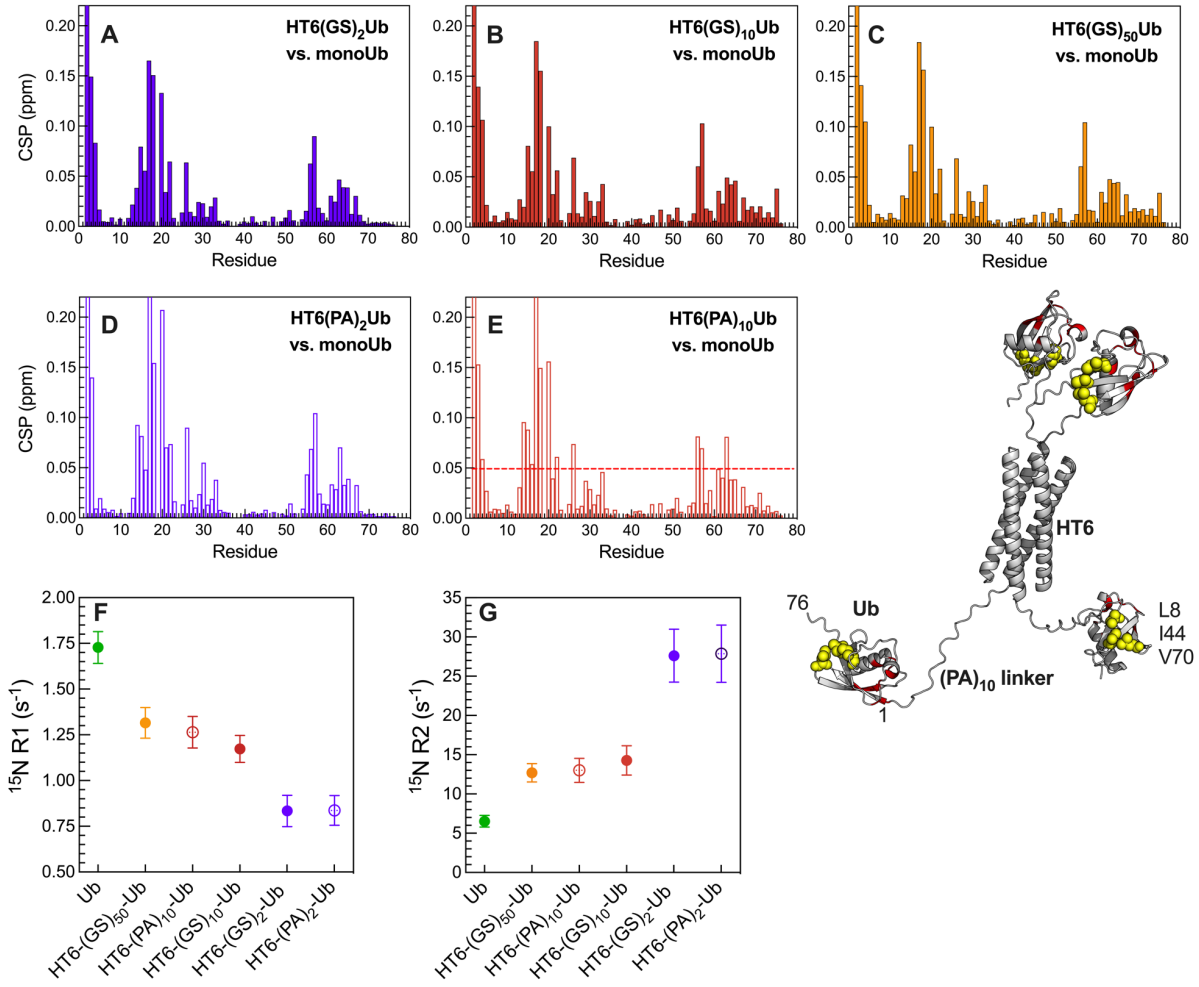

Figure S5. Comparison of Ub amide chemical shift perturbations (CSPs) for resonances in (A) HT6-$(GS)_2$-Ub, (B) HT6-$(GS)_{10}$-Ub, (C) HT6-$(GS)_{50}$-Ub, (D) HT6-$(PA)_2$-Ub, (E) HT6-$(PA)_{10}$-Ub vs. monoUb. CSPs > 0.05 ppm for (E) were mapped onto representative HT6-$(PA)_{10}$-Ub structure (see Fig. 2B) showing that only resonances spatially near the linker were perturbed, while not impacting the hydrophobic patch of Ub (yellow spheres). (F, G) Average ^{15}N R_1 and R_2 relaxation rates for Ub resonances in secondary structure organized in terms of decreasing R_1 and increasing R_2 rates. Error bars denote standard deviation of residue-specific relaxation rates (>63 residues used) per construct.

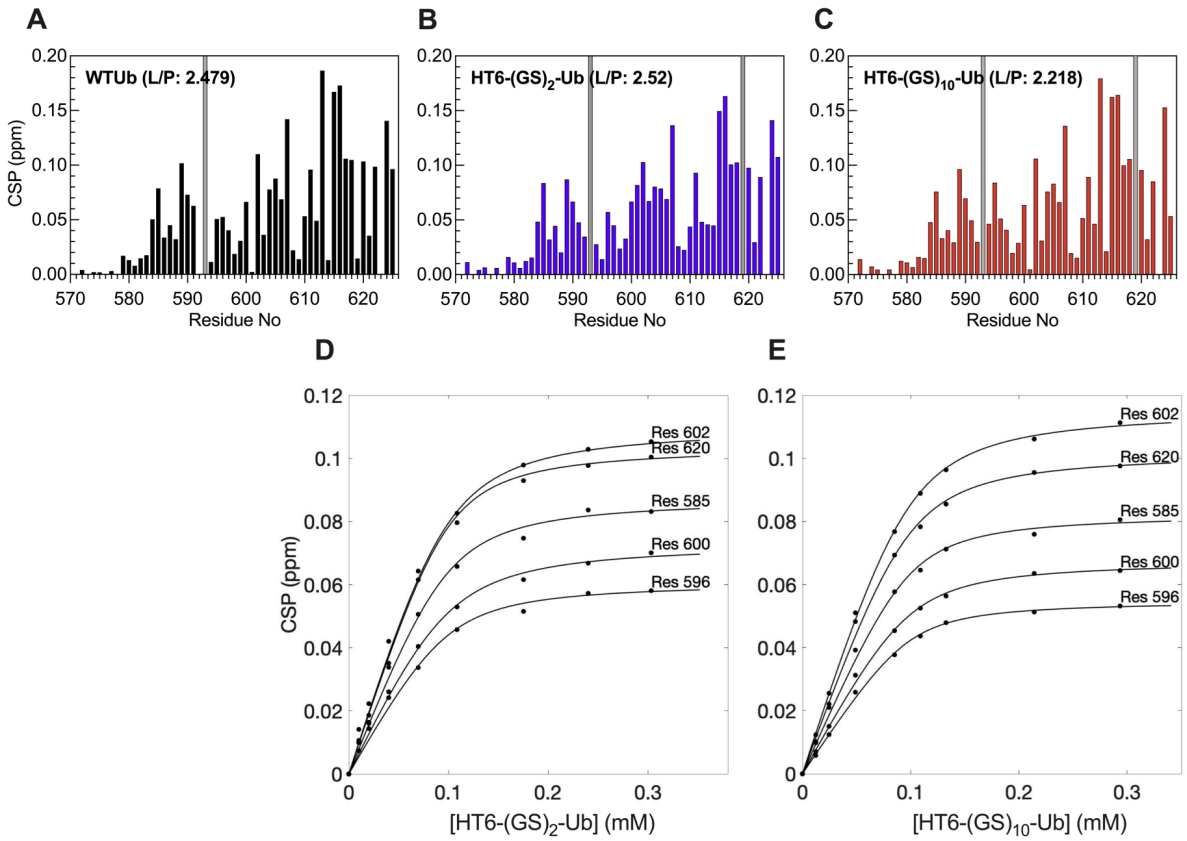

Figure S6. Comparison of backbone amide CSPs for UBA UBQLN2 (100 μM) upon titration with (A) WT Ub (ligand:protein (L:P=2.48), (B) HT6-GS_2-Ub (L:P=2.52) & (C) HT6-GS_{10}-Ub (L:P=2.22). Gray bars mark the resonances that are completely attenuated at the end of the titration. (D,E) Residue-specific amide titration curves of (D) HT6-$(GS)_2$-Ub, and (E) HT6-$(GS)_{10}$-Ub. Here fits from a single-site binding model were superpositioned on experimental data points.

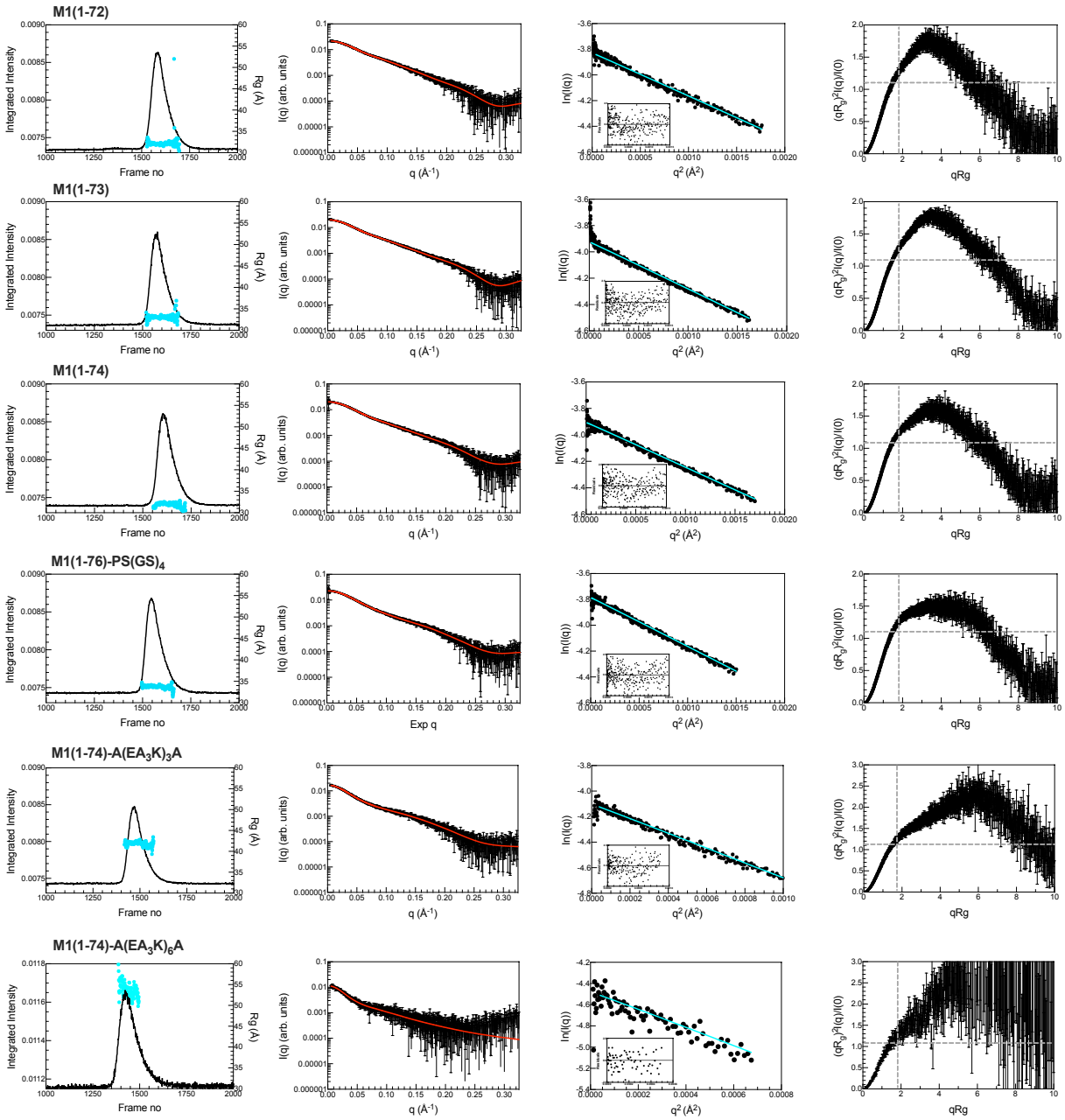

Figure S7. SEC-SAXS profiles for M1(1-72), M1(1-73), M1(1-74), M1(1-76)-PS(GS)$_4$, M1(1-74)-A(EA$_3$K)$_3$A & M1(1-74)-A(EA$_3$K)$_6$A. I(q) vs. q scattering curves (middle left) determined from frames (1580-1586) M1(1-72), (1556-1577) M1(1-73), (1592-1605) M1(1-74), (1540-1551) M1(1-76)-PS(GS)$_4$, (1440-1450) M1(1-74)-A(EA$_3$K)$_3$A, & (1437-1440) M1(1-74)-A(EA$_3$K)$_6$A on the corresponding SEC-SAXS profiles (left). Red line in the I(q) profile indicates fit from P(r) analysis (see Fig. 4). Cyan line in the Guinier plot (middle right) is linear fit of ln(I(q)) vs. q^2, while inset shows residuals of fit. Dimensionless Kratky plots (right) include dashed lines to indicate where a globular protein would peak.

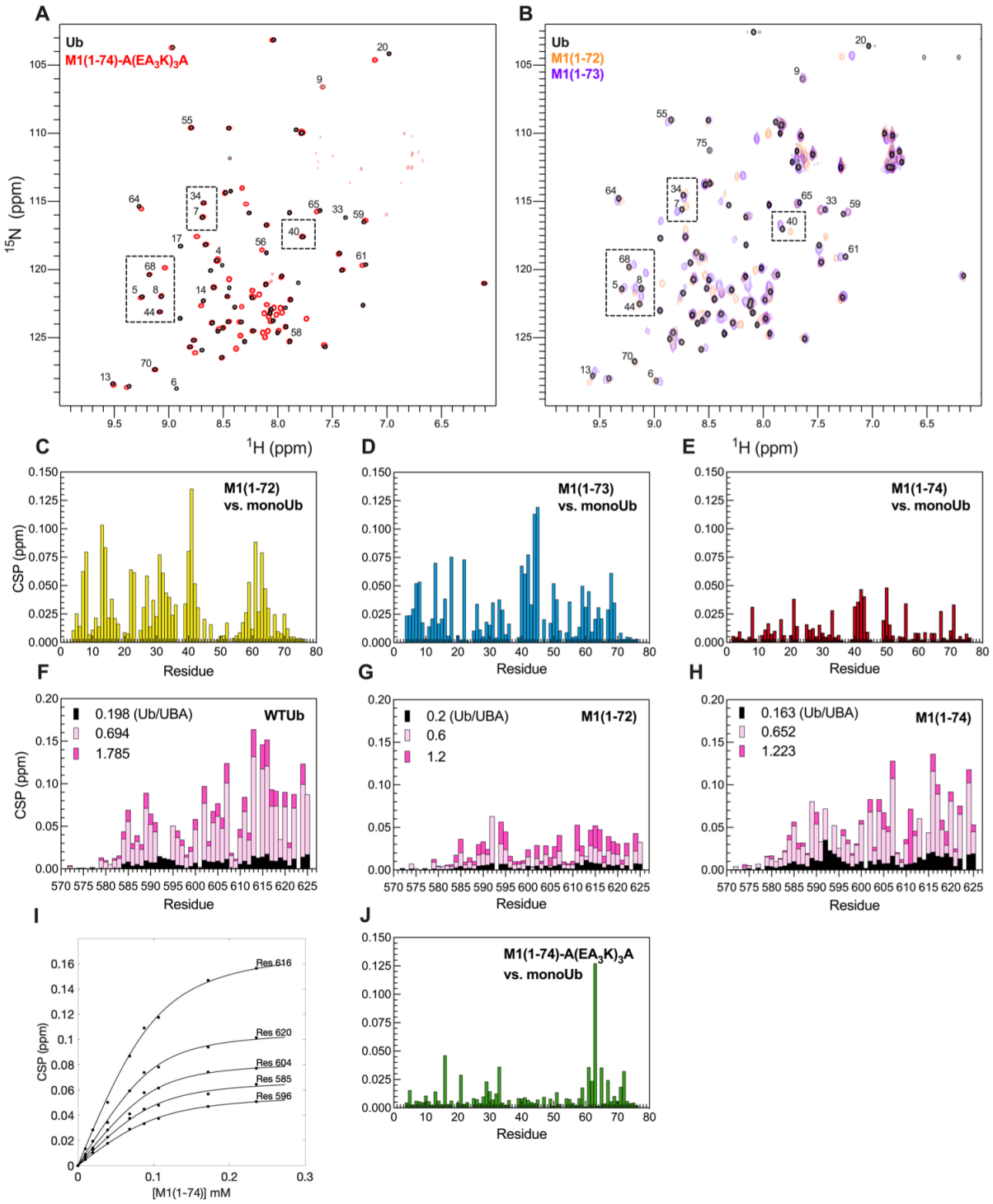

Figure S8. (A) ^{15}N-^{1}H TROSY-HSQC spectra of 200 μM ^{15}N labeled Ub (black) and M1-Ub4 (1-74)-A(EA$_3$K)$_3$A (red). (B) ^{15}N-^{1}H SOFAST-HMQC spectra of 100 μM ^{15}N labeled Ub (black), 200 μM M1-Ub4 (1-72) (orange), and 200 μM M1-Ub4 (1-73) (purple). Natural abundance spectra for M1-Ub4 (1-72) and M1-Ub4 (1-73) were collected with >1024 scans. Spectra were collected at 25 ˚C in 20 mM NaPhosphate buffer pH 6.8. (C, D, E) Chemical shift perturbations (CSPs) measured for backbone amide resonances in (C) M1-Ub4 (1-72), (D) M1-Ub4 (1-73), (E) M1-

Ub4 (1-74) with respect to ^{15}N labeled monoUb resonances under identical buffer conditions. (F, G, H) Amide CSPs measured at three different Ub:^{15}N UBA ratios (as noted in figure) upon titrating unlabeled (F) WT Ub (G) M1-Ub4 (1-72) (H) M1-Ub4 (1-74) into 100 μM ^{15}N UBA UBQLN2. (I) Residue-specific backbone amide titration curves for UBA resonances as unlabeled M1-Ub4 (1-74) was titrated into 100 μM ^{15}N UBA UBQLN2. Single-site binding model (black line) was fit to residue-specific titration curves (data points) to obtain K_d values. (J) Chemical shift perturbations (CSPs) measured for backbone amide resonances in M1(1-74)-A$(EA_3K)_3$A with respect to ^{15}N labeled monoUb resonances under identical buffer conditions. As we observed multiple resonances for select Ub residues in M1(1-72), M1(1-73), M1(1-74) & M1(1-74)-A$(EA_3K)_3$A, the largest CSP values for each residue are reported here.

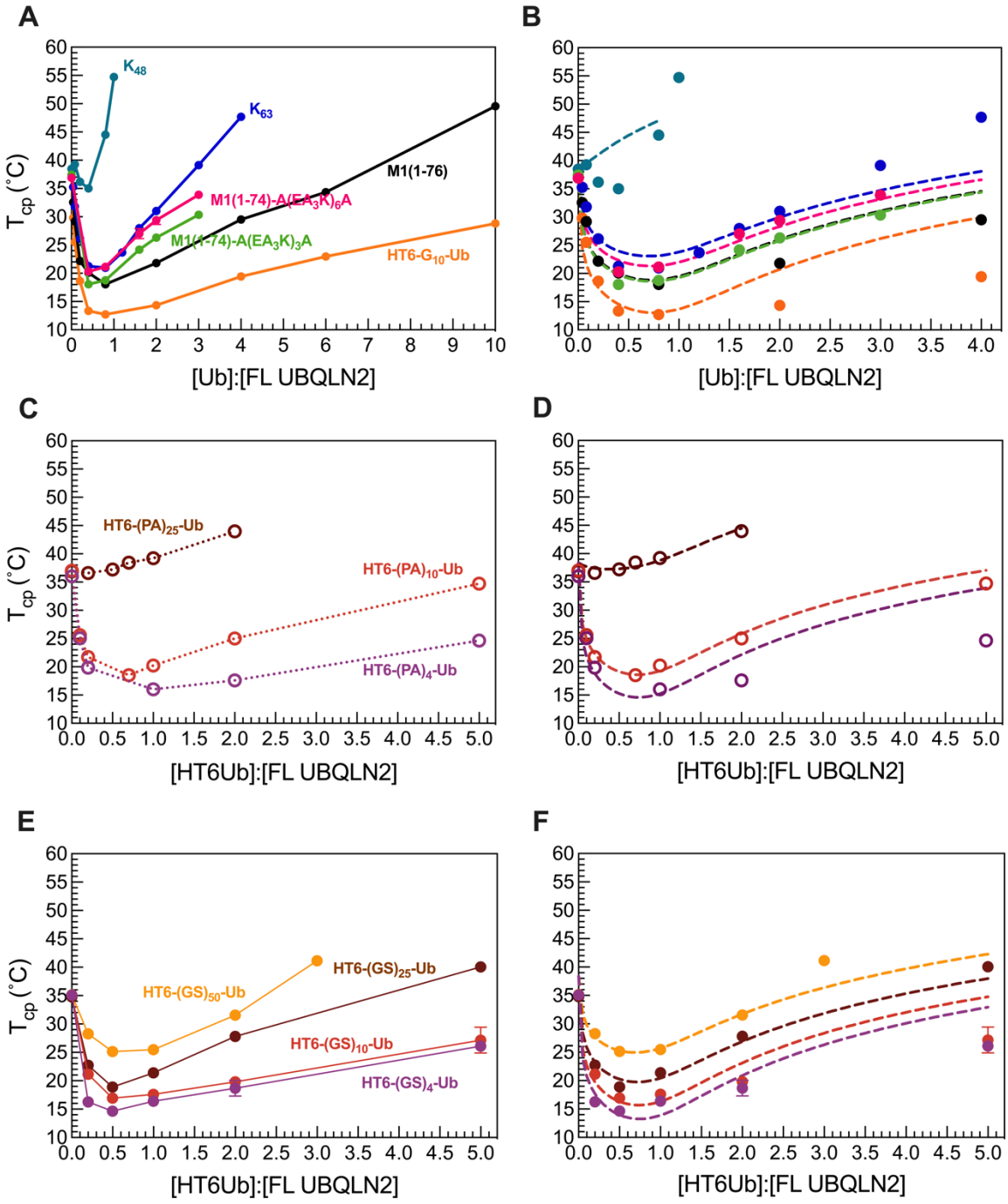

Figure S9. There is an optimal ligand architecture of polyUb that maximizes full-length (FL) UBQLN2 phase separation. (A, C) Experimental cloud point temperature curves of FL UBQLN2 with natural and designed polyUb chains of different linkages. FL UBQLN2 concentration was kept constant at 30 μM. (B, D) Analytical theory fitted to experimental data.

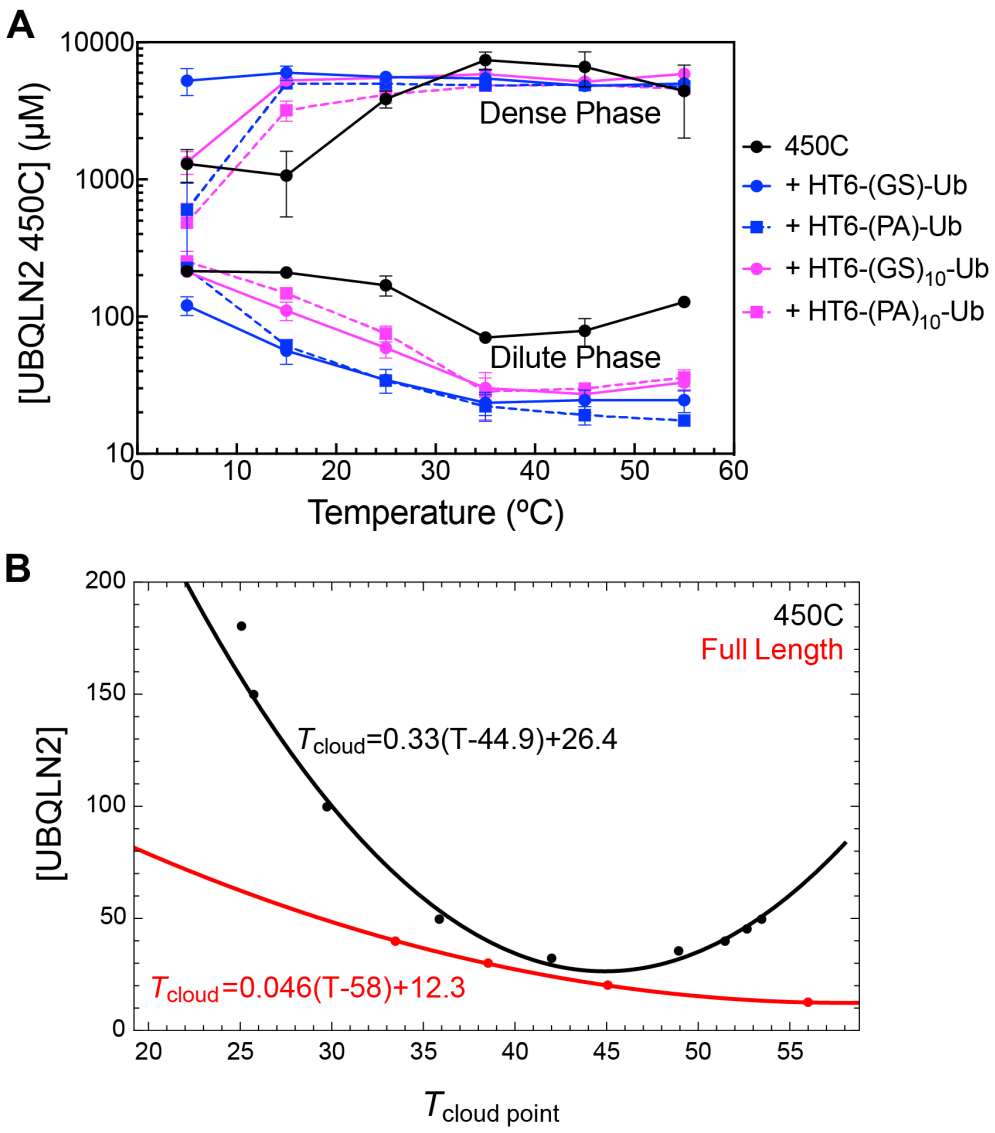

Figure S10. (A) Dilute and dense phase measurements of 450C in the presence of different HT6-Ub ligands as a function of temperature. Initial protein concentrations of 250 μM 450C and 250 μM HT6-Ub ligand were used (i.e., a 1:1 450C:Ub ratio). Average concentrations from n=3 measurements with error bars reflecting the standard deviation. (B) Comparison of experimental cloud point measurements (points) and fits to Eq. S13 for full length UBQLN2 (red) and 450C variant of UBQLN2 (black). Data for full length UBQLN2 and 450C variant of UBQLN2 are from (19) and (20), respectively.

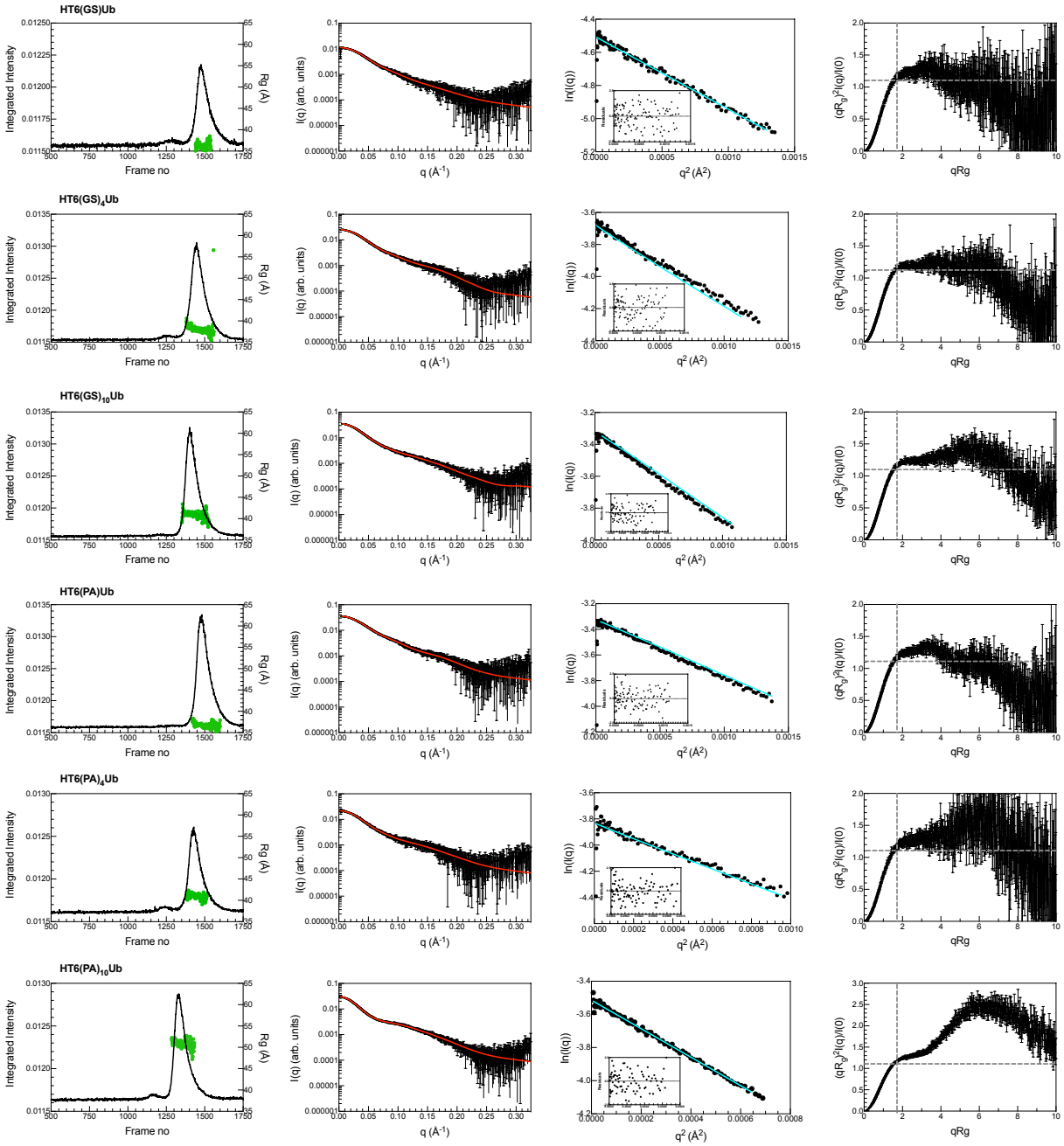

Figure S11. (A) SEC-SAXS profiles for HT6-(GS)-Ub, HT6-$(GS)_4$-Ub, HT6-$(GS)_{10}$-Ub, HT6-(PA)-Ub, HT6-$(PA)_4$-Ub, & HT6-$(PA)_{10}$-Ub collected in 20 mM phosphate buffer pH 6.8 with 200 mM NaCl, 0.5 mM EDTA & 0.02 % NaAz. I(q) vs. q scattering curves (middle left) determined from frames (1455-1513) HT6-(GS)-Ub, (1459-1482) HT6-$(GS)_4$-Ub, (1387-1408) HT6-$(GS)_{10}$-Ub, (1473-1484) HT6-(PA)-Ub, (1418-1428) HT6-$(PA)_4$-Ub & (1314-1354) HT6-$(PA)_{10}$-Ub on the corresponding SEC-SAXS profiles (left). Red line in the I(q) profile indicates fit from P(r) analysis. Cyan line in the Guinier plot (middle right) is the linear fit of ln(I(q)) vs. q^2, while inset shows residuals of fit. Dimensionless Kratky plots (right) include dashed lines to indicate where a globular protein would peak.

D. SI Tables

Table S1. Calculated average binding affinity (K_d) values of UBQLN2 UBA domain with WT Ub, Ub mutants, HT6-$(GS)_2$/$(GS)_{10}$-Ub and M1(1-74) used in the study. The errors represent the standard deviation of K_d values determined from multiple NMR resonances as listed below (see Fig. S1).

Protein	K_d (μM)	Amino acid resonances used in K_d determination
WT Ub	2.6 ± 0.3	584, 585, 589, 590, 591, 596, 600, 602, 604, 605, 606, 607, 610, 611, 613, 615, 616, 617, 618, 620, 622, 624
V70I	6.0 ± 0.9	585, 589, 591, 593, 600, 602, 604, 605, 606, 607, 611, 614, 615, 616, 617, 618, 619, 620, 621, 622, 624
V70A	7.4 ± 0.6	589, 590, 596, 600, 602, 604, 605, 606, 607, 610, 612, 615, 616, 617, 618, 620, 624
I44V	13.6 ± 1.2	585, 589, 590, 593, 595, 596, 600, 602, 604, 605, 606, 607, 611, 612, 614, 615, 616, 617, 618, 619, 620, 622, 624
V70I/I44V	39 ± 3.6	588, 591, 596, 600, 606, 622
V70A/I44V	59 ± 1.8	589, 590, 596, 602, 604, 605, 606, 607, 610, 611, 612, 614, 615, 616, 618, 620, 622, 624
I44A	> 1000	
HT6-$(GS)_2$-Ub	11.7 ± 2.1	585, 590, 596, 600, 602, 604, 605, 607, 610, 616, 617, 618, 619, 620, 622, 624
HT6-$(GS)_{10}$-Ub	9.0 ± 1.5	585, 589, 590, 591, 595, 596, 600, 602, 604, 605, 606, 607, 610, 611, 613, 615, 616, 617, 619, 620, 622, 624
M1(1-74)-Ub4	15.6 ± 3.8	585, 596, 600, 602, 604, 606, 607, 615, 616, 617, 618, 620, 622, 624

Table S2. Structural parameters of HT6-Ub and M1 series from SAXS data analysis. Indicated in parentheses are the methods/software used for R_g analysis. [a]R_g and errors were determined from the linear fit of ln(I(q)) vs. q^2 and [b]R_g and errors were determined from choosing multiple values of D_{max}. Data collected in 20 mM sodium phosphate buffer pH 6.8 with 0.5 mM EDTA and 0.02 % NaN_3.

Construct	R_g (Å)[a] (Guinier) [a]	R_g (Å)[b] (GNOM) [b]	D_{max} (Å) (GNOM)
HT6-(GS)-Ub	37.10 ± 0.06	38.19 ± 0.09	140
HT6-$(GS)_2$-Ub	36.75 ± 0.17	38.08 ± 0.19	137
HT6-$(GS)_4$-Ub	37.65 ± 0.07	38.89 ± 0.10	143
HT6-$(GS)_{10}$-Ub	39.74 ± 0.12	41.37 ± 0.14	148
HT6-$(GS)_{25}$-Ub	47.02 ± 0.62	51.01 ± 0.66	193
HT6-$(GS)_{50}$-Ub	56.31 ± 0.09	58.70 ± 0.15	227
HT6-(PA)-Ub	36.98 ± 0.09	38.12 ± 0.08	129
HT6-$(PA)_2$-Ub	38.03 ± 0.24	39.88 ± 0.26	150
HT6-$(PA)_4$-Ub	40.80 ± 0.06	42.00 ± 0.06	144
HT6-$(PA)_{10}$-Ub	50.52 ± 0.13	52.29 ± 0.20	184
HT6-$(PA)_{25}$-Ub	62.61 ± 0.23	66.24 ± 0.36	249
M1(1-72)	32.03 ± 0.11	34.09 ± 0.15	125
M1(1-73)	33.09 ± 0.07	35.08 ± 0.12	128
M1(1-74)	32.21 ± 0.09	33.76 ± 0.11	122
M1(1-76)	32.42 ± 0.03	34.22 ± 0.21	140
M1(1-76)-PS$(GS)_4$	34.04 ± 0.10	35.73 ± 0.17	139
M1(1-74)-A$(EA_3K)_3$A	42.06 ± 0.19	45.25 ± 0.40	182
M1(1-74)-A$(EA_3K)_6$A	51.84 ± 1.18	56.19 ± 1.42	212
HT6-(GS)-Ub, 200 mM NaCl	36.16 ± 0.18	37.75 ± 0.12	126
HT6-$(GS)_4$-Ub, 200 mM NaCl	37.77 ± 0.14	38.73 ± 0.14	128
HT6-$(GS)_{10}$-Ub, 200 mM NaCl	41.16 ± 0.13	42.32 ± 0.14	142
HT6-(PA)-Ub, 200 mM NaCl	36.85 ± 0.12	37.81 ± 0.14	124
HT6-$(PA)_4$-Ub, 200 mM NaCl	41.05 ± 0.26	42.67 ± 0.24	147
HT6-$(PA)_{10}$-Ub, 200 mM NaCl	50.78 ± 0.16	52.81 ± 0.21	190

Table S3. Inclusion energy values for 450C UBQLN2 & FL UBQLN2 with polyUb ligands (related to Figure 4I, 4J).

Ligand	Inclusion energy (kT)	
	450C UBQLN2	FL UBQLN2
HT6-(GS)-Ub	9.43	-
HT6-$(GS)_2$-Ub	9.83	-
HT6-$(GS)_4$-Ub	10.07	6.67
HT6-$(GS)_{10}$-Ub	10.78	7.07
HT6-$(GS)_{25}$-Ub	11.47	7.79
HT6-$(GS)_{50}$-Ub	13.24	8.80
HT6-(PA)-Ub	9.65	-
HT6-$(PA)_2$-Ub	9.73	-
HT6-$(PA)_4$-Ub	10.16	6.89
HT6-$(PA)_{10}$-Ub	11.35	7.58
HT6-$(PA)_{25}$-Ub	14.13	11.84
M1(1-73)	10.89	-
M1(1-74)	9.78	-
M1(1-76)	10.01	7.62
M1(1-76)-$PS(GS)_4$	9.81	-
M1(1-74)-$A(EA_3K)_3A$	10.52	7.58
M1(1-74)-$A(EA_3K)_6A$	11.15	8.08
K48-Ub4	-	14.52
K63-Ub4	-	8.42

Table S4. Constructs used in the study

Construct	Sequence
HT6-G_{10}-Ub	MTLREIEELLRKIIEDSVRSVAELEDIEKWLKKIGGGGGGGGGG MQIFVKTLTGKTITLEVEPSDTIENVKAKIQDKEGIPPDQQRLIFAGKQLEDGRTLSDYNIQ KESTLHLVLRLRGG
HT6-G_{10}-Ub V70I	MTLREIEELLRKIIEDSVRSVAELEDIEKWLKKIGGGGGGGGGGMQIFVKTLTGKTITLEV EPSDTIENVKAKIQDKEGIPPDQQRLIFAGKQLEDGRTLSDYNIQKESTLHLILRLRGG
HT6-G_{10}-Ub V70A	MTLREIEELLRKIIEDSVRSVAELEDIEKWLKKIGGGGGGGGGG MQIFVKTLTGKTITLEVEPSDTIENVKAKIQDKEGIPPDQQRLIFAGKQLEDGRTLSDYNIQ KESTLHLALRLRGG
HT6-G_{10}-Ub I44V	MTLREIEELLRKIIEDSVRSVAELEDIEKWLKKIGGGGGGGGGGMQIFVKTLTGKTITLEV EPSDTIENVKAKIQDKEGIPPDQQRLVFAGKQLEDGRTLSDYNIQKESTLHLVLRLRGG
HT6-G_{10}-Ub I44A	MTLREIEELLRKIIEDSVRSVAELEDIEKWLKKIGGGGGGGGGGMQIFVKTLTGKTITLEV EPSDTIENVKAKIQDKEGIPPDQQRLAFAGKQLEDGRTLSDYNIQKESTLHLVLRLRGG
HT6-G_{10}-Ub V70I/I44V	MTLREIEELLRKIIEDSVRSVAELEDIEKWLKKIGGGGGGGGGGMQIFVKTLTGKTITLEV EPSDTIENVKAKIQDKEGIPPDQQRLVFAGKQLEDGRTLSDYNIQKESTLHLILRLRGG
HT6-G_{10}-Ub V70A/I44V	MTLREIEELLRKIIEDSVRSVAELEDIEKWLKKIGGGGGGGGGGMQIFVKTLTGKTITLEV EPSDTIENVKAKIQDKEGIPPDQQRLVFAGKQLEDGRTLSDYNIQKESTLHLALRLRGG
HT6-GS-Ub	MTLREIEELLRKIIEDSVRSVAELEDIEKWLKKIGSMQIFVKTLTGKTITLEVEPSDTIENVK AKIQDKEGIPPDQQRLIFAGKQLEDGRTLSDYNIQKESTLHLVLRLRGG
HT6-$(GS)_2$-Ub	MTLREIEELLRKIIEDSVRSVAELEDIEKWLKKIGSGSMQIFVKTLTGKTITLEVEPSDTIEN VKAKIQDKEGIPPDQQRLIFAGKQLEDGRTLSDYNIQKESTLHLVLRLRGG
HT6-$(GS)_4$-Ub	MTLREIEELLRKIIEDSVRSVAELEDIEKWLKKIGSGSGSGSMQIFVKTLTGKTITLEVEPS DTIENVKAKIQDKEGIPPDQQRLIFAGKQLEDGRTLSDYNIQKESTLHLVLRLRGG
HT6-$(GS)_{10}$-Ub	MTLREIEELLRKIIEDSVRSVAELEDIEKWLKKIGSGSGSGSGSGSGSGSGSGSMQIFVK TLTGKTITLEVEPSDTIENVKAKIQDKEGIPPDQQRLIFAGKQLEDGRTLSDYNIQKESTLH LVLRLRGG
HT6-$(GS)_{25}$-Ub	MTLREIEELLRKIIEDSVRSVAELEDIEKWLKKIGSGSGSGSGSGSGSGSGSGSGSGSG SGSGSGSGSGSGSGSGSGSGSGSGSMQIFVKTLTGKTITLEVEPSDTIENVKAKIQDKE GIPPDQQRLIFAGKQLEDGRTLSDYNIQKESTLHLVLRLRGG
HT6-$(GS)_{50}$-Ub	MTLREIEELLRKIIEDSVRSVAELEDIEKWLKKIGSGSGSGSGSGSGSGSGSGSGSGSG SGSGSGSGSGSGSGSGSGSGSGSGSGSGSGSGSGSGSGSGSGSGSGSG SGSGSGSGSGSGSGSGSGSMQIFVKTLTGKTITLEVEPSDTIENVKAKIQDKEGIPPD QQRLIFAGKQLEDGRTLSDYNIQKESTLHLVLRLRGG
HT6-PA-Ub	MTLREIEELLRKIIEDSVRSVAELEDIEKWLKKIPAMQIFVKTLTGKTITLEVEPSDTIENVK AKIQDKEGIPPDQQRLIFAGKQLEDGRTLSDYNIQKESTLHLVLRLRGG
HT6-$(PA)_2$-Ub	MTLREIEELLRKIIEDSVRSVAELEDIEKWLKKIPAPAMQIFVKTLTGKTITLEVEPSDTIEN VKAKIQDKEGIPPDQQRLIFAGKQLEDGRTLSDYNIQKESTLHLVLRLRGG

HT6-$(PA)_4$-Ub	MTLREIEELLRKIIEDSVRSVAELEDIEKWLKKIPAPAPAPAMQIFVKTLTGKTITLEVEPSD TIENVKAKIQDKEGIPPDQQRLIFAGKQLEDGRTLSDYNIQKESTLHLVLRLRGG
HT6-$(PA)_{10}$-Ub	MTLREIEELLRKIIEDSVRSVAELEDIEKWLKKIPAPAPAPAPAPAPAPAPAMQIFVKTL TGKTITLEVEPSDTIENVKAKIQDKEGIPPDQQRLIFAGKQLEDGRTLSDYNIQKESTLHLV LRLRGG
HT6-$(PA)_{25}$-Ub	MTLREIEELLRKIIEDSVRSVAELEDIEKWLKKIPAPAPAPAPAPAPAPAPAPAPAPAPA PAPAPAPAPAPAPAPAPAPAPAMQIFVKTLTGKTITLEVEPSDTIENVKAKIQDKEGIPPD QQRLIFAGKQLEDGRTLSDYNIQKESTLHLVLRLRGG
M1-Ub4 (1-72)	MQIFVKTLTGKTITLEVEPSDTIENVKAKIQDKEGIPPDQQRLIFAGKQLEDGRTLSDYNIQK ESTLHLVLRMQIFVKTLTGKTITLEVEPSDTIENVKAKIQDKEGIPPDQQRLIFAGKQLEDGR TLSDYNIQKESTLHLVLRMQIFVKTLTGKTITLEVEPSDTIENVKAKIQDKEGIPPDQQRLIFA GKQLEDGRTLSDYNIQKESTLHLVLRMQIFVKTLTGKTITLEVEPSDTIENVKAKIQDKEGIP PDQQRLIFAGKQLEDGRTLSDYNIQKESTLHLVLRLRGG
M1-Ub4 (1-73)	MQIFVKTLTGKTITLEVEPSDTIENVKAKIQDKEGIPPDQQRLIFAGKQLEDGRTLSDYNIQK ESTLHLVLRLMQIFVKTLTGKTITLEVEPSDTIENVKAKIQDKEGIPPDQQRLIFAGKQLEDG RTLSDYNIQKESTLHLVLRLMQIFVKTLTGKTITLEVEPSDTIENVKAKIQDKEGIPPDQQRLI FAGKQLEDGRTLSDYNIQKESTLHLVLRLMQIFVKTLTGKTITLEVEPSDTIENVKAKIQDKE GIPPDQQRLIFAGKQLEDGRTLSDYNIQKESTLHLVLRLRGG
M1-Ub4 (1-74)	MQIFVKTLTGKTITLEVEPSDTIENVKAKIQDKEGIPPDQQRLIFAGKQLEDGRTLSDYNIQK ESTLHLVLRLRMQIFVKTLTGKTITLEVEPSDTIENVKAKIQDKEGIPPDQQRLIFAGKQLED GRTLSDYNIQKESTLHLVLRLRMQIFVKTLTGKTITLEVEPSDTIENVKAKIQDKEGIPPDQQ RLIFAGKQLEDGRTLSDYNIQKESTLHLVLRLRMQIFVKTLTGKTITLEVEPSDTIENVKAKIQ DKEGIPPDQQRLIFAGKQLEDGRTLSDYNIQKESTLHLVLRLRGG
M1-Ub4 (1-76)	MQIFVKTLTGKTITLEVEPSDTIENVKAKIQDKEGIPPDQQRLIFAGKQLEDGRTLSDYNIQK ESTLHLVLRLRGGMQIFVKTLTGKTITLEVEPSDTIENVKAKIQDKEGIPPDQQRLIFAGKQL EDGRTLSDYNIQKESTLHLVLRLRGGMQIFVKTLTGKTITLEVEPSDTIENVKAKIQDKEGIP PDQQRLIFAGKQLEDGRTLSDYNIQKESTLHLVLRLRGGMQIFVKTLTGKTITLEVEPSDTI ENVKAKIQDKEGIPPDQQRLIFAGKQLEDGRTLSDYNIQKESTLHLVLRLRGG
M1(1-76)-PS$(GS)_4$ (linker in orange)	MQIFVKTLTGKTITLEVEPSDTIENVKAKIQDKEGIPPDQQRLIFAGKQLEDGRTLSDYNIQK ESTLHLVLRLRGGPSGSGSGSGSMQIFVKTLTGKTITLEVEPSDTIENVKAKIQDKEGIPPD QQRLIFAGKQLEDGRTLSDYNIQKESTLHLVLRLRGGPSGSGSGSGSMQIFVKTLTGKTIT LEVEPSDTIENVKAKIQDKEGIPPDQQRLIFAGKQLEDGRTLSDYNIQKESTLHLVLRLRGG PSGSGSGSGSMQIFVKTLTGKTITLEVEPSDTIENVKAKIQDKEGIPPDQQRLIFAGKQLED GRTLSDYNIQKESTLHLVLRLRGG
M1(1-74)- A$(EA_3K)_3$A (linker in orange)	MQIFVKTLTGKTITLEVEPSDTIENVKAKIQDKEGIPPDQQRLIFAGKQLEDGRTLSDYNIQK ESTLHLVLRLRAEAAAKEAAAKEAAAKAMQIFVKTLTGKTITLEVEPSDTIENVKAKIQDKEG IPPDQQRLIFAGKQLEDGRTLSDYNIQKESTLHLVLRLRAEAAAKEAAAKEAAAKAMQIFVK TLTGKTITLEVEPSDTIENVKAKIQDKEGIPPDQQRLIFAGKQLEDGRTLSDYNIQKESTLHL VLRLRAEAAAKEAAAKEAAAKAMQIFVKTLTGKTITLEVEPSDTIENVKAKIQDKEGIPPDQ QRLIFAGKQLEDGRTLSDYNIQKESTLHLVLRLRGG
M1(1-74)- A$(EA_3K)_6$A (linker in orange)	MQIFVKTLTGKTITLEVEPSDTIENVKAKIQDKEGIPPDQQRLIFAGKQLEDGRTLSDYNIQKE STLHLVLRLRAEAAAKEAAAKEAAAKEAAAKEAAAKEAAAKAMQIFVKTLTGKTITLEVEPSD TIENVKAKIQDKEGIPPDQQRLIFAGKQLEDGRTLSDYNIQKESTLHLVLRLRAEAAAKEAAAK EAAAKEAAAKEAAAKEAAAKAMQIFVKTLTGKTITLEVEPSDTIENVKAKIQDKEGIPPDQQRL IFAGKQLEDGRTLSDYNIQKESTLHLVLRLRAEAAAKEAAAKEAAAKEAAAKEAAAKEAAAKA

	MQIFVKTLTGKTITLEVEPSDTIENVKAKIQDKEGIPPDQQRLIFAGKQLEDGRTLSDYNIQKE STLHLVLRLRGG
UBQLN2 450C	MRAMQALMQIQQGLQTLATEAPGLIPSFTPGVGVGVLGTAIGPVGPVTPIGPIGPIVPFTP IGPIGPIGPTGPAAPPGSTGSGGPTGPTVSSAAPSETTSPTSESGPNQQFIQQMVQALA GANAPQLPNPEVRFQQQLEQLNAMGFLNREANLQALIATGGDINAAIERLLGSQPSW

Table S5. SASSIE parameters and results for generation of ligand hub conformational ensembles

Ligand hub	Flexible component of starting structure	Structures Generated	Accepted	Best single structure (reduced χ^2)	Number of structures with lowest χ^2
HT6-$(PA)_4$-Ub	35-42, 115-118	30000	20613	2.77	83 $\chi^2 < 4$
HT6-$(PA)_{10}$-Ub	35-54,126-129	30000	18786	1.06	13 $\chi^2 < 1.5$
M1-Ub4 (1-72)	72-73, 144-145, 216-217, 288-292	30000	13449	0.86	44 $\chi^2 < 1.0$
M1-Ub4 (1-74)	72-74, 146-148, 220-222, 294-298	30000	18927	1.03	47 $\chi^2 < 1.5$
M1-Ub4 (1-74) $A(EA_3K)_6A$	72-76, 105-107, 178-182, 211-213, 284-288, 317-319, 390-394	30000	19359	0.63	140 $\chi^2 < 0.75$

E. Legends for Datasets

Dataset. SEC-MALS-SAXS Data Collection and Analysis for all Ub hubs in this study. There are two tabs (Dataset 1A, Dataset 1B) within this dataset file. Dataset 1A contains all information pertinent to HT6-Ub ligand hubs, and Dataset 1B refers to information about M1-based polyUb ligand hubs. See attached Excel XLSX file.

F. SI References

1. C. A. Castañeda, *et al.*, Linkage via K27 Bestows Ubiquitin Chains with Unique Properties among Polyubiquitins. *Structure* **24**, 423–436 (2016).

2. P. Raymond-Smiedy, B. Bucknor, Y. Yang, T. Zheng, C. A. Castañeda, "A Spectrophotometric Turbidity Assay to Study Liquid-Liquid Phase Separation of UBQLN2 In Vitro" in *Protein Aggregation: Methods and Protocols*, Methods in Molecular Biology., A. S. Cieplak, Ed. (Springer US, 2023), pp. 515–541.

3. T. P. Dao, *et al.*, Ubiquitin Modulates Liquid-Liquid Phase Separation of UBQLN2 via Disruption of Multivalent Interactions. *Mol. Cell* **69**, 965-978.e6 (2018).

4. F. Delaglio, *et al.*, NMRPIPE - A multidimensional spectral processing system based on UNIX pipes. *J Biomol NMR* **6**, 277–293 (1995).

5. W. F. Vranken, *et al.*, The CCPN data model for NMR spectroscopy: Development of a software pipeline. *Proteins Struct. Funct. Bioinforma.* **59**, 687–696 (2005).

6. J. B. Hall, D. Fushman, Characterization of the overall and local dynamics of a protein with intermediate rotational anisotropy: Differentiating between conformational exchange and anisotropic diffusion in the B3 domain of protein G. *J. Biomol. NMR* **27**, 261–275 (2003).

7. D. Fushman, S. Cahill, D. Cowburn, The main-chain dynamics of the dynamin pleckstrin homology (PH) domain in solution: analysis of 15N relaxation with monomer/dimer equilibration. *J. Mol. Biol.* **266**, 173–194 (1997).

8. N. Kirby, *et al.*, Improved radiation dose efficiency in solution SAXS using a sheath flow sample environment. *Acta Crystallogr. Sect. Struct. Biol.* **72**, 1254–1266 (2016).

9. D. Franke, C. M. Jeffries, D. I. Svergun, Correlation Map, a goodness-of-fit test for one-dimensional X-ray scattering spectra. *Nat. Methods* **12**, 419–422 (2015).

10. J. B. Hopkins, R. E. Gillilan, S. Skou, BioXTAS RAW: improvements to a free open-source program for small-angle X-ray scattering data reduction and analysis. *J. Appl. Crystallogr.* **50**, 1545–1553 (2017).

11. V. Piiadov, E. Ares de Araújo, M. Oliveira Neto, A. F. Craievich, I. Polikarpov, SAXSMoW 2.0: Online calculator of the molecular weight of proteins in dilute solution from experimental SAXS data measured on a relative scale. *Protein Sci.* **28**, 454–463 (2019).

12. R. P. Rambo, J. A. Tainer, Accurate assessment of mass, models and resolution by small-angle scattering. *Nature* **496**, 477–481 (2013).

13. D. I. Svergun, Determination of the regularization parameter in indirect-transform methods using perceptual criteria. *J. Appl. Crystallogr.* **25**, 495–503 (1992).

14. J. E. Curtis, S. Raghunandan, H. Nanda, S. Krueger, SASSIE: A program to study intrinsically disordered biological molecules and macromolecular ensembles using experimental scattering restraints. *Comput. Phys. Commun.* **183**, 382–389 (2012).

15. M. Mirdita, *et al.*, ColabFold: making protein folding accessible to all. *Nat. Methods* **19**, 679–682 (2022).

16. J. Wyman, S. J. Gill, Ligand-Linked Phase Changes in a Biological System: Applications to Sickle Cell Hemoglobin. *Proc. Natl. Acad. Sci. U. S. A.* **77**, 5239–5242 (1980).

17. J. Wyman, *Binding and Linkage: Functional Chemistry of Biological Macromolecules* (University Science Books, 1990) (July 23, 2023).

18. M. Rubinstein, R. H. Colby, *Polymer Physics* (OUP Oxford, 2003).

19. T. P. Dao, *et al.*, Mechanistic insights into enhancement or inhibition of phase separation by different polyubiquitin chains. *EMBO Rep.* **23**, e55056 (2022).

20. Y. Yang, H. B. Jones, T. P. Dao, C. A. Castañeda, Single Amino Acid Substitutions in Stickers, but Not Spacers, Substantially Alter UBQLN2 Phase Transitions and Dense Phase Material Properties. *J. Phys. Chem. B* **123**, 3618–3629 (2019).